Resonant Raman scattering in GaN single crystals and GaN-based heterostructures: feasibility for laser cooling

Yujie J. Ding* **and Jacob B. Khurgin**

[1]*Department of Electrical and Computer Engineering, Lehigh University, Bethlehem, PA 18015, USA*

[2]*Department of Electrical and Computer Engineering, The Johns Hopkins University, Baltimore, MD 21218, USA*

**Corresponding author: yud2@lehigh.edu*

Received November 23, 2012; accepted December 13, 2012; posted online January 6, 2013

The recent progress on Raman scattering in GaN single crystals and GaN/AlN heterostructures is reviewed. Anti-Stokes Raman scattering is used to determine electron-phonon scattering time and decay time constant for longitudinal-optical phonons. In a typical high electron mobility transistor based on GaN/AlN heterostructures, strong resonances are reached for the first-order and second-order Raman scattering processes. Therefore, both Stokes and anti-Stokes Raman intensities are dramatically enhanced. The feasibility for laser cooling of a nitride structure is studied. A further optimization will enable us to reach the threshold for laser cooling. Raman scattering have potential applications in up-conversion lasers and laser cooling of nitride ultrafast electronic and optoelectronic devices.

OCIS codes: 190.5650, 190.7220.

doi: 10.3788/COL201311.011901.

1. Introduction

When a semiconductor material is pumped in the vicinity of its direct bandgap, a number of different radiative processes may take place with energy of the emitted photons being either below (Stokes) or above (anti-Stokes) the energy of the pump photon[1]. As demanded by the energy conservation, in case of the Stokes process there is a net transfer of energy from the photons to the semiconductor whereas in the case of the anti-Stokes process the energy is transferred from the semiconductor to the photons. Since the energy of the semiconductor vibrations is quantized in the form of acoustic and optical phonons, one customarily talks of phonon emission for the Stokes processes and phonon absorption for the anti-Stokes ones. Since photons do not interact directly with the lattice there are always intermediate states-free and bound electron-hole pair states that mediate the process. Depending on nature of the mediating states one differentiates between processes supported by real states-photoluminescence (PL) and virtual states-Raman scattering[2].

The considered Raman process creates a virtual electron–hole pair, i.e. the pair energy is uncertain[1]. According to the uncertainty principle, the probability of creating the virtual pair is inversely proportional to the square of the "energy defect" (detuning) and the virtual electron or hole get instantly scattered by a single optical phonon with a small wave vector and then instantly recombine. It is worth noting that no real state is created due to the nature of a virtual process, and therefore, there can be no spontaneous recombination. If the optical phonon is emitted, the scattered Stokes Raman photon is red-shifted. If the phonon is absorbed, the scattered anti-Stokes Raman photon is blue shifted. Thus the two telltale signs distinguishing the Raman process are the spectrum that closely replicated the pump spectrum and only modified by the phonon lifetime broadening and the fact that there is no time lag between the pump and Raman phonons. Indeed, Raman is a virtual process occurring on the time scale of being proportional to the inverse frequency detuning, which is much shorter than phase coherence time. The polarization at the pump frequency is created and then it is scattered into the polarization at the Stokes or anti-Stokes frequency before the polarization decays, i.e. it is faster than the phase coherence time. It is important for us to understand that Raman is a coherent process for one photon-phase is preserved in a sense that it is transferred to phonon and Stokes photon-but because we have many phonons we end up with the averaging effect.

Strictly speaking, Raman scattering should be thought of as coherent process, but only in the sense that the phase of incoming photon should be preserved as the combined phase of the scattered Stokes photon and the emitted optical phonon. But since the observer cannot possibly see the phase of a phonon, the phase shift between pump and Raman scattered photons is completely randomized. In other words, the scattered photon (Stokes or anti-Stokes) faithfully remembers the energy and arrival time of the pump photon but the memory of the phase is completely obliterated due to uncertainty of the phonon phase[1,3].

In general, Raman scattering have potential applications in up-conversion lasers[4] and laser cooling of glasses[5] and semiconductors[6−9]. Since these processes can remove longitudinal-optical (LO) phonons, it can certainly improve the performance of GaN-based ultrafast electronic and optoelectronic devices. Indeed, as the density of the LO phonons is greatly decreased, the scattering rate of electrons by the phonons is significantly reduced. In addition, the heat generated through the decay of LO phonons is also decreased. Among different semiconductor materials, GaN-based heterostructures and crystals may be superior for achieving efficient removal of LO phonons and laser cooling. Indeed, the LO phonon energy for GaN is about 91.8 meV, which is one of the highest among different semiconductor materials. As a result, phonon removal and laser cooling could be

 © 2013 Chinese Optics Letters

achieved even at room temperature since the bandtail absorption can be minimized by, e.g. setting the photon energy of the incoming laser beam to one LO phonon energy below the bandgap of GaN[10].

When the photon energy of the anti-Stokes Raman signal is close to the bandgap of the nitride material, it may be difficult for us to separate the anti-Stokes Raman signal from the anti-Stokes PL. One effective method for us to discriminate the former process from the latter is to investigate the dependence of the emission peak on the pump wavelength or lattice temperature. Indeed, for the anti-Stokes Raman scattering the photon energy of the emission peak shifts with the pump photon energy. However, it is independent of the lattice temperature. It is important for us to note that in both cases the anti-Stokes shifts are equal to the LO phonon energy within the experimental errors. In comparison, for the anti-Stokes PL, the peak photon energy does not usually shift with the pump photon energy or lattice temperature.

GaN is a wide band gap material characterized by a parabolic lowest conduction band separated by 1.4 eV from the nearest satellite valley. It is also characterized by a high energy of LO phonons (i.e., 91.8 meV). These properties make GaN an ideal candidate for high electron mobility transistors (HEMTs) capable of operating at high powers and elevated temperatures. Rule-of-thumb considerations predict that electron velocity saturation in GaN should occur near the onset of strong emission of LO phonons, i.e., when the kinetic energy of electrons becomes comparable to 91.8 meV. The primary mechanism for the velocity saturation is the accumulation of the hot LO phonons, which leads to additional power dissipation[11−13], and therefore, the corresponding electronic devices will deteriorate in time. The saturation velocity should then be of the order of 3×10^7 cm/s. This assumption is supported by the Monte Carlo simulations, but the measured electron drift velocity in microwave GaN-based transistors rarely surpasses 1.5×10^7 cm/s. To understand the reasons for this discrepancy, let us consider distinct properties of GaN separating it from, say, GaAs. In GaAs, the cation and anion do not differ much in masses and electron affinities, while in GaN, they differ by a large amount. A strong polar bond in GaN raises phonon frequencies with a large splitting between LO and transverse optical (TO) branches and increases electron scattering by polar optical phonons by at least an order of magnitude in comparison to GaAs. At the same time, the large mismatch between the ion masses in GaN causes substantial splitting between the energies of optical and acoustic branches, such that the zone center LO phonon energy is larger than the highest LA or TA energies by a factor of higher than 2[14]. Unlike GaAs, the traditional Klemens channel for decay of an LO phonon into two acoustic phonons is energy-forbidden. As a result, the LO phonon lifetime is increased to a few picoseconds. The combination of fast emission of LO phonons and long phonon lifetimes results in a large nonequilibrium population of the LO phonons.

Due to the Fröhlich interaction, it takes no more than 100 fs for an electron to emit one LO phonon in GaN[15−17]. Indeed, using time-resolved backward Raman scattering spectroscopy, the electron-LO-phonon emission time was previously determined to be (50±10) fs[16], which is close to the theoretical estimate of 10 fs. Another approach to deduce the LO-phonon emission time for an electron is to balance the LO-phonon scattering loss per electron[18,19] and the relaxation rate of the excess energy of the electron system in time domain. Using such a method the LO-phonon emission time was determined to be 200 fs[20]. Under a direct current (dc) electric field, the power loss per electron through its collision with the LO phonon is approximately equal to the power gain per electron drifting under a dc electric field. Therefore, the LO-phonon emission time was also deduced for an n-GaN metal-semiconductor field effect transistor[21]. It is worth noting that most of the previous investigations[16,20,21] were focused on the bulk-GaN structures. In contrast, the time constant for the decay of the emitted LO phonons into TO and acoustic phonons[22] is 2.8 ps[23] (see Fig. 1). Even if GaN is pumped below its bandgap, such a constant was measured by us to be 4.2 ps (see section 2 below). Since the LO phonons generated by electrons are accumulated, phonon occupancies are elevated[24], i.e. the non-equilibrium or hot phonons are induced. Previously, the hot-phonon temperature and lifetime were estimated from a biased AlGaN/AlN channel based on microwave noise technique[24]. Among different techniques, Raman scattering may be one of the most direct techniques for investigating hot phonons based on the previous result[25].

Recently, we investigated the hot phonon effect on electron-velocity saturation in GaN[26]. We showed that electron velocity at high electric fields is reduced due to heating of electron gas since the high density of non-equilibrium LO phonons cannot efficiently transfer heat to the acoustic phonons that can then carry it to the thermal bath or heat sink. Even though the GaN-based HEMT may be the next-generation microwave power amplifiers with the possibilities of handling high powers as well as operating within a wide bandwidth[27], hot LO phonons could impose a fundamental limit to the performance of a GaN-based HEMT. Indeed, as mentioned above the accumulation of the LO phonons emitted by the electrons drifting in a HEMT may cause the device characteristics to deteriorate.

The hot electrons were generated in a biased AlN/GaN HEMT in PL measurements[17]. They were produced as a result of the Fröhlich interaction between the long-lived LO phonons and the electrons drifting in the HEMT and also determine the LO phonon emission time. An

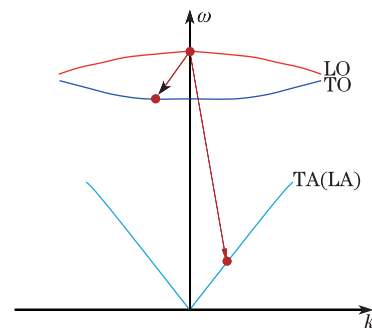

Fig. 1. Primary decay channels of near-zone-center LO phonons in GaN.

electric field present in a GaN/AlN heterostructure can bring both the first-order and second-order Raman scattering processes into strong resonances[28]. The resonant Stokes and anti-Stokes Raman scatterings result in the increase and decrease in non-equilibrium LO phonon temperatures, respectively.

In this paper, we hope to familiarize the reader with the most recent advances in using Raman processes to improve the performance of photonic and electronic devices based on highly polar III-V semiconductor GaN and its alloys.

This paper is organized as follows. In section 2, we review the recent results on the Raman scattering when the nitride structure is pumped below or above its bandgap. In section 3, we review the results on Raman scattering when the pump photon energies are tuned across the bandgap. In section 4, we discuss the feasibility for laser cooling of a nitride structure. We draw concluding remarks in section 5.

2. Raman scattering below or above bandgap

Below the bandgap of GaN, Murugkar *et al.* investigated second-order Stokes Raman spectroscopy of GaN films grown on sapphire substrates when they were pumped at 488 nm[29]. Second-order Raman spectra were measured to probe the continuum of phonon pairs with their wave vectors of equal magnitude but opposite directions. Two-phonon spectra were dominated by contributions due to LO phonons. Behr *et al.* studied Stokes and anti-Stokes Raman scattering on GaN films grown on sapphire substrates at the pump photon energies of 3.00 and 3.05 eV, respectively[30]. By heating up the GaN films from 300 to 870 K, they significantly reduced the bandgap of the GaN films. As a result, the Stokes Raman signals were dramatically enhanced as the temperature was increased. After the Raman signals were corrected for the temperature-dependent occupation probabilities, they deduced the resonance profiles for the Stokes one-phonon and two-phonon Raman scattering. As the temperature was increased, the Stokes Raman signals were enhanced by one order of magnitude. These dramatic increases were caused by the close-bandgap-resonance enhancements. However, even at the highest temperature of 870 K, the anti-Stokes scattering intensity of the second-order phonon spectrum was too weak for making an accurate quantitative analysis. It is worth noting, though, when the excitation photon energy is 3.54 eV, which is above the bandgap of GaN at room temperature, even four-LO-phonon signals were observable at room temperature. However, the signal for the four-LO-phonon Raman scattering is two orders of magnitude lower than one-LO-phonon Raman scattering.

In order to directly measure electron-LO-phonon scattering rates, Tsen *et al.* investigated subpiconsecond time-resolved Raman spectroscopy in an undoped wurtzite GaN sample grown on a sapphire substrate[31]. The laser pulses used as pump and probe beams were generated by the frequency doubling of a dye laser with the pulse width of 600 fs. The photon energy used in their experiment was around 4.36 eV such that upon the absorption of the pump beam, pairs of electrons and holes were generated with their kinetic energies being about 1 eV. These photogenerated electrons lost their energies by emitting non-equilibrium LO phonons through the Fröhlich interaction. Through the Raman scattering of the probe beam by the non-equilibrium LO phonons, anti-Stokes backward-propagating Raman signal was measured as a function of the time delay between the pump and probe pulses. As a result, the decay time for the LO phonons was measured to be 5 ps at 25 K after simulating the transient dynamics of the coupled carrier-phonon system. As the temperature was increased from 25 to 300 K, the decay time was decreased from 5 to 2.8 ps, by using exactly the same technique[23]. On the other hand, using ultrariolet (UV) laser pulses generated by a frequency-quadrupled mode-locked Ti-sapphire laser with the pulse width being set between 50 fs and 2 ps, anti-Stokes backward-propagating Raman signal was measured as a function of the time delay between the pump and probe pulses[16]. By using an electron cascade model, the electron-LO-phonon scattering time was determined to be 50 fs at 25 K by fitting the data.

We measured the decay time for the LO phonons by employing pump-probe technique. The wavelengths for the pump and probe beams are both 380 nm, i.e., below the bandgap of the GaN film. Their pump width is 2 ps. The average powers for the pump and probe beams are 138 and 10 mW, respectively. We measured the Raman signal as a function of the delay time for each pump pulse relative to the corresponding probe pulse. According to Fig. 2, the decay time for the LO phonons is deduced to be around 4.2 ps. This value is consistent with 2.8 ps measured on a single GaN crystal[22].

3. Raman scattering across bandgap

In this subsection, we review our result on Stokes and anti-Stokes Raman scattering on a GaN/AlN heterostructure[28]. Indeed, an electric field present in a GaN/AlN heterostructure can bring both the first-order and second-order Raman scattering processes into strong resonances. The resonant Stokes and anti-Stokes Raman scattering results in the increase and decrease of non-equilibrium LO phonon temperatures, respectively. Moreover, the phonon temperature measured from the Raman scattering is increased with an applied electric

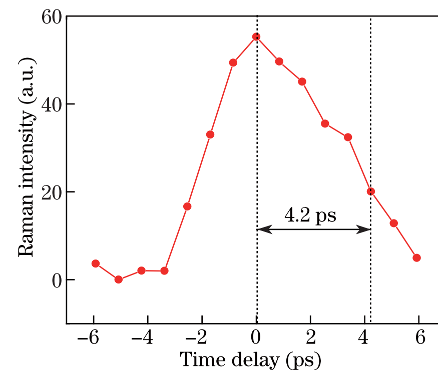

Fig. 2. Raman signal is measured as a function of time delay for each pump pulse relative to corresponding probe pulse in GaN film.

field at a much higher rate than the lattice temperature due to the presence of field-induced non-equilibrium LO phonons.

Our GaN/AlN heterostructure was grown by molecular beam epitaxy. A 200-nm-thick unintentionally-doped GaN layer was grown on the top of a 3-μm-thick semi-insulating GaN layer, which was first deposited on the top of the 300-μm sapphire substrate. Subsequently, the GaN layer was capped by a 4-nm-thick AlN layer. High-density two-dimensional electrons were confined within the GaN layer next to the GaN/AlN interface[32]. Source and drain ohmic contacts were formed by the evaporation of the gold film followed by annealing. The gate was measured to be 30 μm in length. At room temperature, the electron sheet concentration and mobility were measured to be 2.5×10^{13} cm^{-2} and 1 200 cm^2/(V·s), respectively.

A Raman signal scattered by the AlN side of the HEMT backward was collected by a two-stage cascaded monochromator at room temperature (295 K) at different biases applied between the source and drain in the range of 0–36 V. The outgoing Raman signal was then measured using a photomultiplier tube after going through the monochromator. A coherent picoseconds radiation with the output wavelength in the range of 369–385 nm, produced by frequency-doubling a mode-locked picoseconds Ti:sapphire laser output in a 10-mm-thick BBO crystal, was used as an incident beam. The width of each incident pulse was measured to be 3 ps. During each measurement, a typical average incident power of 30 mW was used. The incident beam was focused down to the HEMT with a beam radius of ∼150 μm. The lattice temperature of the HEMT under a fixed bias was deduced by fitting the PL spectral profiles on the low-energy side, generated by a picoseconds coherent UV

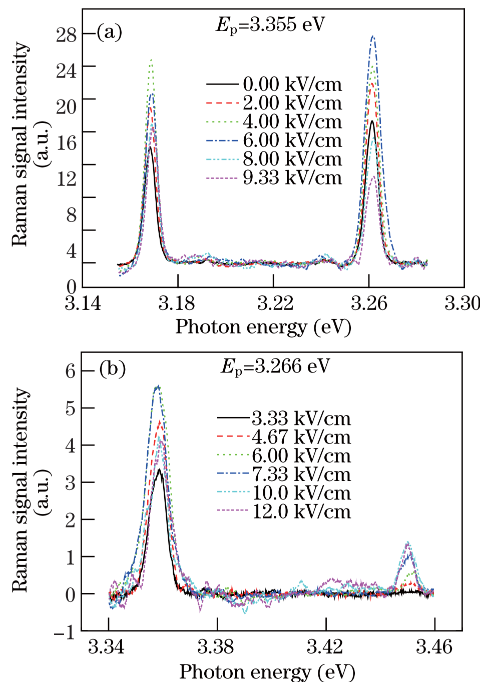

Fig. 3. Spectra of the first-order and the second-order (a) Stokes and (b) anti-Stokes Raman scattering at different electric fields indicated. $E_{\rm i}$ is used to designate the photon energy of the incident beam.

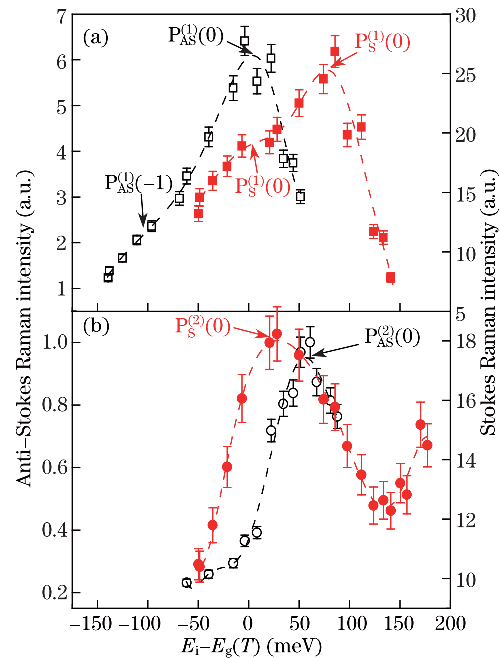

Fig. 4. Dependences of (a) the first-order and (b) the second-order Raman-scattering signal intensities deduced from Fig. 3, on the photon energy of the incident beam measured relative to the bandgap of GaN. Filled squares and filled circles: Stokes; open squares and open circles: anti-Stokes. All dashed curves correspond to fitting to data. Errors are indicated in the figures.

radiation, by using Boltzmann distribution[33]. As a result, we obtained the bandgap, $E_{\rm g}(T)$, for the GaN channel at each fixed dc electric field. Using Ref. [34], we deduced the corresponding DC lattice temperature.

The temperatures of the LO phonons are determined as

$$T_{\rm 1LO}=\frac{\eta\omega_{\rm LO}}{k_{\rm B}\ln[(n^{(1)}+1)/n^{(1)}]},\qquad(1)$$

where $n^{(1)}$ is the phonon occupation number for the first-order Raman scattering[25]. The two peaks resolved in Fig. 3 correspond to the first-order and second-order Raman scattering of the incident pulses by the LO phonons with their energies being $\eta\omega_{\rm LO}\approx 91.8$ meV in the GaN channel layer[28]. At different electric fields or incident photon energies the intensities for the first-order and second-order Stokes and anti-Stokes Raman scattering are different (see Fig. 4). Each of the four Raman scattering processes is going through its own resonance at a specific electric field.

One can see from Fig. 4 that for the first-order Raman scattering there are two dominant peaks labeled by $P_{\rm AS}^{(1)}(0)$ and $P_{\rm S}^{(1)}(1)$ corresponding to the anti-Stokes and Stokes Raman scattering at $E_{\rm i}-E_{\rm g}\approx 3$ meV and $E_{\rm i}-E_{\rm g}\approx 80$ meV, respectively. According to Ref. [34], these two peaks correspond to the resonances for the incoming and outgoing photons to the bandgap of the GaN channel, respectively. A tail $P_{\rm AS}^{(1)}(-1)$ and a shoulder $P_{\rm S}^{(1)}(0)$ can be attributed to the anti-Stokes and Stokes Raman scattering at $E_{\rm i}-E_{\rm g}\approx -96$ meV and $E_{\rm i}-E_{\rm g}\approx 0$ meV, respectively. They correspond to the resonances of the outgoing and incoming photon energies to the bandgap, respectively. The resonance for the incoming photons

$P_{\rm S}^{(1)}(0)$ is much weaker than that for the outgoing photons $P_{\rm S}^{(1)}(1)$. For the resonance of the outgoing photons, free excitons are generated by the incoming photons, which further enhance the Raman signal intensities (i.e. a double resonance). For the first-order anti-Stokes Raman scattering, however, the resonance for the incoming photons $P_{\rm AS}^{(1)}(0)$ is much stronger than that for the outgoing photons $P_{\rm AS}^{(1)}(-1)$. Such behaviors are quite different from Ref. [35]. In our heterostructure the generation of the electrons and their subsequent drift in a dc electric field have further enhanced $P_{\rm AS}^{(1)}(0)$ and $P_{\rm S}^{(1)}(1)$.

One can see from Fig. 4(b) that for the second-order Raman scattering two resonant peaks, labeled as $P_{\rm S}^{(2)}(0)$ and $P_{\rm AS}^{(2)}(0)$, are located at $E_{\rm i}-E_{\rm g}(T)\approx 27$ meV and $E_i-E_{\rm g}(T)\approx 56$ meV, respectively. In our experiment, without applying a bias to the GaN/AlN heterostructure, we could not observe any second-order anti-Stokes Raman signal regardless of the detuning. After applying a relatively high electric field, the second-order anti-Stokes Raman peak becomes obvious. Moreover, the Raman signal can be significantly enhanced as the electric field is further increased (see Fig. 3). Such an enhancement caused by the increase of the electric field is an evidence for the presence of the hot phonons. For the second-order Raman scattering, two LO phonons must be absorbed or emitted simultaneously. The increase in the Raman signal intensity starting at $E_{\rm i}-E_{\rm g}(T)\approx 150$ meV in Fig. 4 could be caused by a resonant peak for the Stokes Raman scattering at $E_{\rm i}-E_{\rm g}(T)\approx 184$ meV (i.e., twice the LO phonon energy).

Using Eq. (1), we have determined the phonon temperatures from the first-order Raman scattering[28]. For the incident photon energies of 3.355 and 3.266 eV, the phonon temperature increases at almost the same rate as the lattice temperature for the electric fields in the range of 0–5.33 kV/cm (see Fig. 5). Within such a range the increase of the electric field results in the increase of the lattice temperature, and therefore, the increase the phonon temperature. Above 5.33 kV/cm, however, the increase in the phonon temperature is much steeper than that in the lattice temperature (see Fig. 5). This implies that in such a range the increase in the electric field leads to the generation of additional LO phonons within 3 ps above those determined from the thermal equilibrium at the lattice temperature. Assuming that an electron is accelerated from zero kinetic energy to $\eta\omega_{\rm LO}$ under an electric field of $E_{\rm dc}$, one can then estimate the duration of the acceleration to be 0.86 ps. This value is in the same order of magnitude as the decay time constant for the LO phonons[23]. Therefore, the LO phonons generated by the drifting electrons are excessively accumulated. Based on our experimental result (Fig. 5), the highest phonon temperature is determined to be 1 290 K at the electric field of 11.3 kV/cm, which is higher than the lattice temperature by 583 K.

According to Fig. 3, the photon energy of each emission peak is more or less independent of the applied electric field and therefore lattice temperature. A closer examination of each peak in Fig. 3 indicates that the corresponding anti-Stokes energy shift is equal to the LO phonon energy within our experimental error. Therefore,

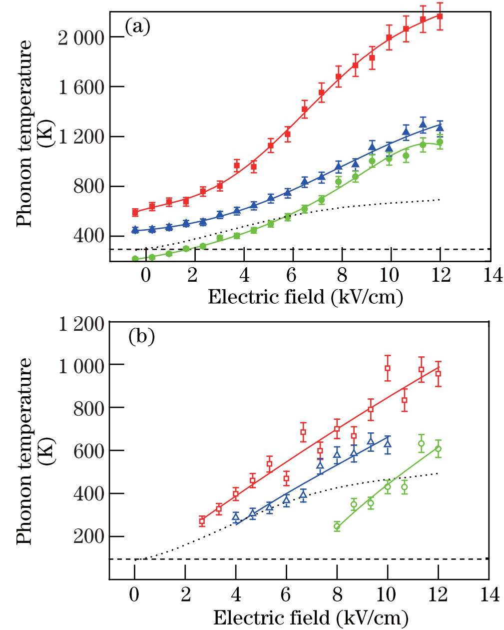

Fig. 5. LO photon temperatures versus electric field, deduced from (a) the first-order (filled symbols) and (b) the second-order (open symbols) Raman scattering, as a function of the electric field at three different sets of photon energies for the incident beam: 3.361 and 3.270 eV (filled and open squares); 3.355 and 3.266 eV (filled and open triangles); 3.316 and 3.225 eV (filled and open circles). Solid curves, dotted curves, and horizontal dashed lines correspond to fitting to data, lattice temperatures, and room temperature (i.e., 295 K), respectively. Errors are indicated in the figures.

we have indeed confirmed that all the emission peaks in Fig. 3 originate from the Raman scattering. In comparison, for the anti-Stokes PL, the photon energy of the emission peak is expected to shift with the lattice temperature.

On the other hand, the phonon temperatures determined from the second-order Raman scattering are considerably lower (see Fig. 5(b)). According to Ref. [36], the wave-vectors of the two LO phonons participating in the second-order Raman scattering must obey a simple selection rule of $\vec{q}_1+\vec{q}_2=\vec{k}_{\rm L}-\vec{k}_{\rm S}$ due to conservation of momentum. Therefore, the LO phonons within the entire Brillouin zone participate in such a process. In such a case, the phonon temperature deduced from the second-order Raman scattering represents an average temperature for the LO phonons within the entire Brillouin zone. In contrast, for the first-order Raman scattering only the LO phonons with the proper values of the wave vectors participate in the process since $\vec{q}=\vec{k}_{\rm L}-\vec{k}_{\rm S}$. At a relatively low electric field, the phonon temperature, $T_{\rm 2LO}$, is about the same as the corresponding lattice temperature (see Fig. 5(b)). As the electric field is increased, however, the phonon temperature becomes higher than the lattice temperature. However, it is increased at a rate much lower than that for the first-order Raman scattering (see Fig. 5). The highest phonon temperature is 839 K at the electric field of 9.33 kV/cm. In comparison, the phonon temperature determined from the first-order Raman scattering at the same electric field is 1 110 K.

According to Fig. 5(b), it appears that the rates of the increases in the phonon temperatures are significantly

less than those determined from the first-order Raman scattering. Since two LO phonons are simultaneously absorbed or emitted for the second-order Raman scattering, the temperature determined from the second-order Raman scattering represents an average value over the LO phonons within the entire Brillouin Zone[28]. This is the reason why the increases in the phonon temperatures as the incident photon energies are increased, determined from the second-order Raman scattering, should be much less. According to Fig. 5(b), the lowest electric field measured at which the second-order anti-Stokes Raman peak is observable is decreased as the photon energy is increased, which can be viewed as an evidence on the generation of the hot LO phonons by the picoseconds incident pulses.

Since the effective mass for electrons is much smaller than that for the heavy holes, photogenerated electrons gain much higher kinetic energies than the heavy holes. Consequently, these electrons not only drift under the dc electric field but also emit and absorb LO phonons through the Fröhlich interaction. Besides the interaction between electrons and LO phonons, the collision between electrons brings the electrons to an equilibrium at the electron temperature (T_e). The electron temperature for the nondegenerate electrons, can be determined by fitting each PL intensity spectrum on the high-energy side using the following dependence[19,33]:

$$I_{\rm PL} \propto e^{-(E-E_{\rm g})/kT_{\rm e}}. \qquad (2)$$

For the PL spectrum measured by us at each bias, we have determined the corresponding value of T_e (see Fig. 6). It is worth noting that the hot-electron temperatures obtained by us are in the same order of magnitude as that determined previously[24]. According to Fig 5, the electron temperature is quite close to the lattice temperature for the dc electric field less than 5 kV/cm. Above such a value, however, the electron temperature is significantly higher than the lattice temperature (see Fig. 6). This is due to the fact that as the electric field is increased the kinetic energies of the electrons are increased. These more energetic electrons then emit and absorb more LO phonons. Since the LO-phonon emission time for an electron is much shorter than the decay time of the LO phonons, the LO phonons become accumulated in time, which results in the increase of the phonon temperature. Consequently, the electron temperature is also increased. Under our experimental condition the scattering of the electrons by acoustic phonons is negligible. Therefore, we assume that the dominant mechanism for the energy loss of the electrons at room temperature is the scattering of the electrons by LO phonons. Under such a case, the power-loss per nondegenerate electron is given by[18]

$$P(T_{\rm e})_{\rm LO} = \frac{\eta\omega_{\rm LO}}{\tau_{\rm e-ph}}\left(\frac{e^{(x_0-x_{\rm e})}-1}{e^{(x_0)}-1}\right) \times \left[\frac{(x_{\rm e}/2)^{1/2}e^{x_{\rm e}/2}K_0(x_{\rm e}/2)}{\sqrt{\pi/2}}\right], \qquad (3)$$

where $\eta\omega_{\rm LO} = 91.8$ meV is the LO phonon energy for GaN, $\tau_{\rm e-ph}$ is the LO-phonon emission time for an electron, $x_{\rm e} = \eta\omega_{\rm LO}/k_{\rm B}T_{\rm e}$, and $x_0 = \eta\omega_{\rm LO}/k_{\rm B}T_{\rm l}$ with $k_{\rm B}$ the Boltzmann constant and K_0 is the modified Bessel function of zero order. Under the steady state, the power loss given by Eq. (3) should be approximately equal to the power gain for an electron from the dc electric field. As a result, one can obtain an expression for the dc electric field applied to the HEMT:

$$E_{\rm dc} = \sqrt{P(T_{\rm e})_{\rm LO}/(e\mu_{\rm e})}, \qquad (4)$$

where e is the charge of an electron and μ_e is the mobility of the electrons.

According to Eq. (4), the dc electric field is as a function of τ_{e-ph} whereby T_e and T_l can be replaced by the values deduced from the PL spectra (see Fig. 6). Such a function was then used by us to achieve a nonlinear-least-square fit to the values of the electric fields calculated by the bias applied to the HEMT divided by 30 μm (see Fig. 7). As a result, the LO phonon emission time for an electron was obtained to be on the order of 100 fs. This value lies between those determined based on time-resolved backward Raman scattering spectroscopy (i.e., 50±10 fs)[16] and using a similar approach under the zero electric field (200 fs)[20] for the bulk GaN. Our value of the LO phonon emission time is much higher than the theoretical value of 10 fs. Such a disprepancy may be caused by the screening of electron-phonon interaction due to the presence of the high-density electrons in a two-dimensional (2D) HEMT[37]. The rate of the energy dissipation for the hot electrons is reduced by the re-absorption of the hot phonons[13], which may increase the emission time of the LO phonons.

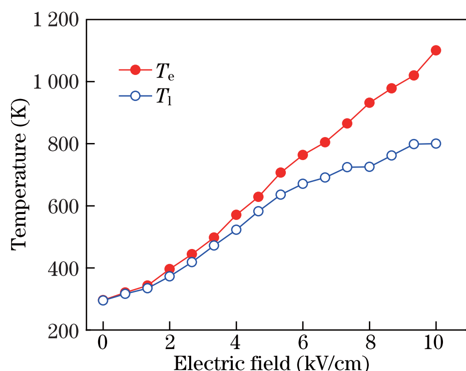

Fig. 6. Electron temperature (filled dots) and lattice temperature (open circles) under different electric fields, deduced from PL spectra.

4. Feasibility for laser cooling

In this subsection, we demonstrate that it is feasible for us to achieve laser cooling of a nitride structure.

We have measured the spectra of the anti-Stokes Raman scattering at room temperature on the GaN film[38,39]. According to Fig. 8, as the pump wavelength is decreased from 389.3 to 370.5 nm, the anti-Stokes Raman peak having the frequency shift of around 740 cm^{-1} (i.e., the scattering of the incoming photons by the A_1 (LO) phonons), is greatly enhanced and then reduced. A closer look of Fig. 8 reveals that at the pump wavelength of 375.8 nm, the Raman signal has the highest amplitude. At such a wavelength, the Raman signal has

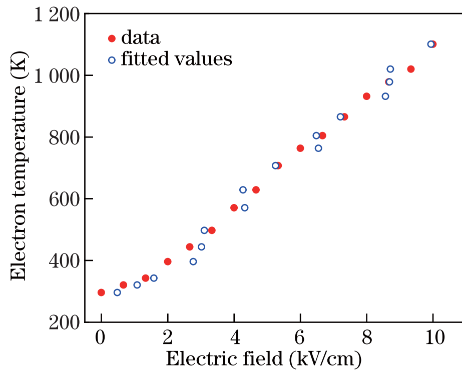

Fig. 7. Electron temperature versus electric field. Data: deduced from the PL spectra; fitted values: after fitting data using Eq. (4).

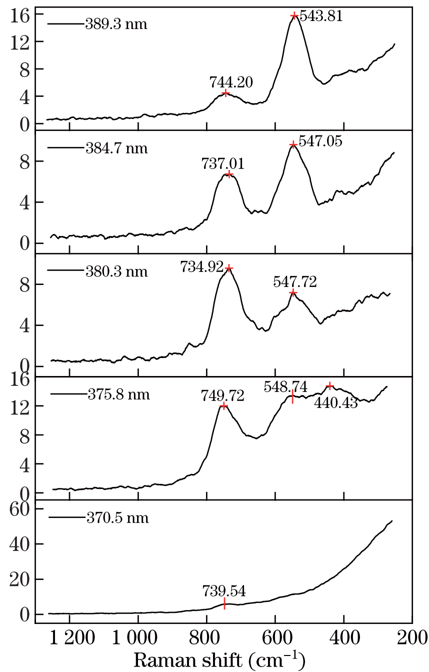

Fig. 8. Spectra of anti-Stokes Raman scattering are measured at different pump wavelengths indicated in the figure at room temperature on a GaN film.

the photon energy of about 3.392 eV. This value is nearly the same as the free-exciton transition energy of 3.387 eV measured by us previously[40]. Therefore, this is our demonstration of the resonance enhancement for the anti-Stokes Raman scattering whereby the outgoing photons strongly resonate to the excition transition. It is worth noting that as the pump wavelength is decreased from 389.3 to 370.5 nm, the wavelength for the emission peak (i.e. the left one in Fig. 8) is correspondingly decreased from 378.3 to 360.6 nm. Such a behavior is used to rule out the contribution to the emission peak due to the anti-Stokes PL. Indeed, for the anti-Stokes PL, the emission wavelength is usually independent of the pump wavelength. According to our result presented in Fig. 8, the anti-Stokes shifts are equal to the LO phonon energy with our experimental error. It indicates that we have maximized the anti-Stokes Raman intensity by optimizing the photon energy of the incoming laser beam. As a result, we have maximized the number of the LO phonons being absorbed. According to Ref. [28], the Stokes Raman scattering reaches the maximum amplitudes at the wavelengths of the incoming photons which are completely different from that for the anti-Stokes Raman scattering. Therefore, it is hopeful for us to eventually achieve the cooling of the GaN film by removing more LO phonons through the anti-Stokes Raman while generating less LO phonons through Stokes Raman scattering.

Besides the spectra of the anti-Stokes Raman scattering, we have also measured the spectra of Stokes Raman scattering at different pump wavelengths, as shown in Fig. 9. It is worth noting that the experimental condition for the investigation of Stokes Raman scattering is exactly the same as that for the anti-Stokes Raman scattering. We have compared the spectra of the Stokes Raman scattering with those of the anti-Stokes Raman scattering. As we expected, the Stokes Raman scattering intensities are relatively higher than those of the anti-Stokes Raman scattering. Figures 8 and 9 reveal that the spectral dependences for the anti-Stokes and Stokes Raman scattering intensities are quite different from each other. Indeed, according to Fig. 10, anti-Stokes and Stokes Raman spectra peak at completely different wavelengths due to different resonant frequencies of the cross sections for the two processes. Based on Fig. 10, the anti-Stokes Raman scattering intensity peaks at 375.8 nm whereas the Stokes Raman scattering intensity is the highest at 370.5 nm. Such significantly different resonance wavelengths are consistent with our previous studies of the anti-Stokes and Stokes resonances made on GaN-based HEMT[28]. According to Fig. 10, at the pump wavelength of 384.7 nm, the Stokes Raman intensity is just a factor of 2.0 higher than the corresponding anti-Stokes Raman intensity. By exploiting the different resonance behaviors of the Stokes and anti-Stokes Raman scattering, the two intensities are quite close to each other at some optimal pump wavelength. By using the InGaN/GaN quantum wells, the optimal pump wavelength is shifted to the visible frequency range. It is obvious that if the anti-Stokes Raman intensity can be enhanced by a factor of just 2.0, the threshold for laser cooling can be reached.

The power conversion efficiency derived from our recent experimental result, i.e. the conversion efficiency from the laser input power to the anti-Stokes Raman output power is 2.3×10^{-6}%. To further improve the efficiency, one can employ high Q microcavities using, e.g. photonic crystals with the modes resonating at both pump and Stokes frequencies. The overall enhancement will be on the order of the square of the finesse of the resonator originating from the increase in the pump power density inside the microcavity and Purcell effect. With an achievable resonator finesse of 1 000, one can then enhance the efficiency to few percent, which may be sufficient for observing laser cooling of the nitride-based HEMTs.

The feasibility study made above indicates that nitride-based microstructures and nanostructures hold great promise for efficient laser cooling.

5. Concluding remarks

We make extensive reviews of the progresses being

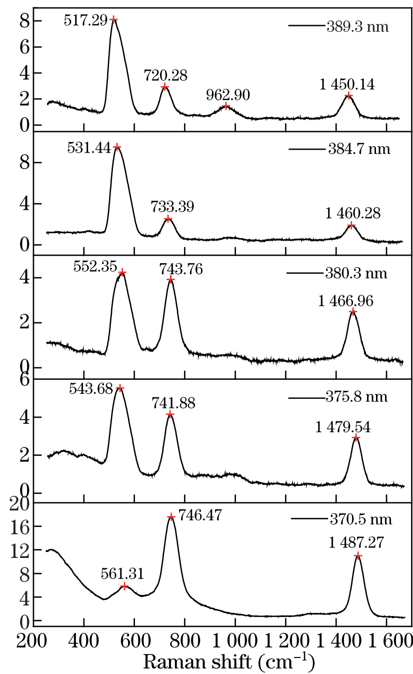

Fig. 9. Spectra of Stokes Raman scattering are measured at different pump wavelengths indicated in the figure at room temperature on a GaN film.

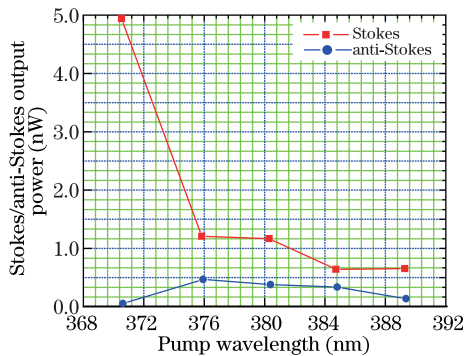

Fig. 10. Spectra of calibrated output powers of Stokes and anti-Stokes Raman signals at room temperature on a GaN film.

made so far on anti-Stokes PL and Stokes and anti-Stokes Raman scattering in GaN single crystals and GaN/AlN heterostructures. Anti-Stokes PL is primarily generated by two-photon absorption, three-photon absorption, and phonon-assisted absorption. On the other hand, anti-Stokes Raman scattering is used to determine electron-phonon scattering time and decay time constant for non-equilibrium LO phonons. In a typical high electron mobility transistor based on GaN/AlN heterostructures, strong resonances are reached for first-order and second-order Raman scattering processes. Therefore, both Stokes and anti-Stokes Raman intensities are dramatically enhanced. We make the feasibility study on laser cooling of a nitride structure.

Raman scattering have potential applications in up-conversion lasers and laser cooling of nitride ultrafast electronic and optoelectronic devices. It is worth noting, though, that other schemes such as isotope disorder of phonons may be used to mitigate hot phonon effects[41].

We are indebted to G. Xu, S. K. Tripathy, X. Mu, K. Wang, Y. Cao, D. Jena, M. Jamil, R. A. Arif, and N. Tansu for their contributions to some of the original results reviewed in this paper. This work was supported by U.S. DARPA.

References

1. P. Y. Yu and M. Cardona, *Fundamentals of Semiconductors*, 3rd Ed. (Springer, NY, 2001).
2. B. E. A. Saleh and M. C. Teich, *Fundamentals of Photonics*, 2nd Ed. (Wiley, NY, 2007).
3. S. Bratos and G. Tarjus, Phys. Rev. A **24,** 1591 (1981).
4. R. Scheps, Prog. Quantum Electron. **20,** 271 (1996).
5. C. W. Hoyt, M. Sheik-Bahae, R. I. Epstein, B. C. Edwards, and J. E. Anderson, Phys. Rev. Lett. **85,** 3600 (2000).
6. M. Sheik-Bahae and R. I. Epstein, Phys. Rev. Lett. **92,** 247403 (2004).
7. J. B. Khurgin, Phys. Rev. Lett. **98,** 177401 (2007).
8. G. Sun, J. B. Khurgin, and R. A. Soref, Appl. Phys. Lett. **90,** 111107 (2007).
9. N. Vermeulen, C. Debaes, P. Muys, and H. Thienpont, Phys. Rev. Lett. **99,** 093903 (2007).
10. J. B. Khurgin, Phys. Rev. B **77,** 235206 (2008).
11. B. K. Ridley, W. J. Schaff, and L. F. Eastman, J. Appl. Phys. **96,** 1499 (2004).
12. C. H. Oxley, M. J. Uren, A. Coates, and D. G. Hayes, IEEE Tran. Electron. Dev. **53,** 565 (2006).
13. M. Ramonas, A. Matulionis, J. Liberis, L. F. Eastman, X. Chen, and Y. J. Sun, Phys. Rev. B **71,** 075324 (2005).
14. H. Harima, J. Phys.: Condens. Matter **14,** R967 (2002).
15. B. K. Ridley, Semicond. Sci. Technol. **4,** 1142 (1989).
16. K. T. Tsen, D. K. Ferry, A. Botchkarev, B. Sverdlov, A. Salvador, and H. Morkoç, Appl. Phys. Lett. **71,** 1852 (1997).
17. S. K. Tripathy, G. Xu, X. Mu, Y. J. Ding, K. Wang, Y. Cao, D. Jena, and J. B. Khurgin, Appl. Phys. Lett. **92,** 013513 (2008).
18. E. M. Conwell, in *High Field Transport in Semiconductors, Solid State Physics, Supplement 9*, Eds. F. Seitz, D. Turnbull, and H. Ehrenreich (Academic, NY, 1967) p. 159.
19. J. Shah, Sol. State Electron. **21,** 43 (1978).
20. H. Ye, G. W. Wicks, and P. M. Fauchet, Appl. Phys. Lett. **74,** 711 (1999).
21. K. Wang, J. Simon, N. Goel, and D. Jena, Appl. Phys. Lett. **88,** 022103 (2006).
22. B. K. Ridley, J. Phys.: Condens. Matter **8,** L511 (1996).
23. K.T. Tsen, D. K. Ferry, A. Botchkarev, B. Sverdlov, A. Salvador, and H. Morkoç, Appl. Phys. Lett. **72,** 2132 (1998).
24. A. Matulionis, J. Liberis, I. Matulioniene, M. Ramonas, L. F. Eastman, J. R. Shealy, V. Tilak, and A. Vertiatchikh, Phys. Rev. B **68,** 035338 (2003).
25. K. T. Tsen, K. R. Wald, T. Ruf, P. Y. Yu, and H. Morkoç, Phys. Rev. Lett. **67,** 2557 (1991).
26. J. Khurgin, Y. J. Ding, and D. Jena, Appl. Phys. Lett. **91,** 252104 (2007).
27. T. Palacios, A. Chakraborty, S. Heikman, S. Keller, S. P. DenBaars, and U. K. Mishra, IEEE Electron Dev. Lett. **27,** 13 (2006).
28. G. Xu, S. K. Tripathy, X. Mu, Y. J. Ding, K. Wang, Y. Cao, D. Jena, and J. B. Khurgin, Appl. Phys. Lett. **93,** 051912 (2008).

29. S. Murukar, R. Merlin, A. Botchkarev, A. Salvador, and H. Morkoç, J. Appl. Phys. **77,** 6042 (1995).
30. D. Behr, J. Wagner, J. Schneider, H. Amano, and I. Akasaki, Appl. Phys. Lett. **68,** 2404 (1996).
31. K. T. Tsen, R. P. Joshi, D. K. Ferry, A. Botchkarev, B. Sverdlov, A. Salvador, and H. Morkoç, Appl. Phys. Lett. **68,** 2990 (1996).
32. Z. Wang, K. Reimann, M. Woerner, T. Elsaesser, D. Hofstetter, J. Hwang, W. J. Schaff, and L. F. Eastman, Phys. Rev. Lett. **94,** 037403 (2005).
33. D. S. Kim and P. Y. Yu, Phys. Rev. B **43,** 4158 (1991).
34. I. Vurgaftman and J. R. Meyer, J. Appl. Phys. **94,** 3675 (2003).
35. J. Reydellet, P. Y. Yu, J. M. Besson, and M. Balkanski, in *Physics of Semiconductors 1978,* Ed. B. L. H. Wilson (Inst. of Phys., Bristol, UK, 1979) pp. 1271-1274.
36. A. G. Cristóbal, A. Cantarero, C. T. Giner, and M. Cardona, Phys. Rev. B **49,** 13430 (1994).
37. A. Matulionis, J. Liberis, M. Ramonas, I. Matulionienè L. F. Eastman, A. Vertiatchikh, X. Chen, and Y.-J. Sun, Phys. Stat. Sol. (c) **7,** 2585 (2005).
38. Y. J. Ding and J. B. Khurgin, *CLEO 2012* QTh4E.2 (2012).
39. Y. J. Ding and J. B. Khurgin, Laser Photon. Rev. **6,** 660 (2012).
40. S. K. Tripathy, G. Xu, X. Mu, Y. J. Ding, M. Jamil, R. A. Arif, and N. Tansu, Appl. Phys. Lett. **93,** 201107 (2008).
41. J. B. Khurgin, D. Jena, and Y. J. Ding, Appl. Phys. Lett. **93,** 032110 (2008).